AIAA 81-1264R

Large-Scale Vortex-Lattice Model for the Locally Separated Flow over Wings

Joseph Katz*
Technion—Israel Institute of Technology, Haifa, Israel

The flowfield over wings with controlled separation was studied by applying a modified vortex-lattice model. Viscous effects were accounted for by vortex-ring modeling of the cellular shapes observed above separated, unswept leading-edge wings. The separation line location for the considered cases was known from experiments; this determined the location of the separated vortex rings and enabled the prediction of wing loading by means of potential theory. Presented calculated results are in agreement with experimental wind tunnel data.

Nomenclature

A_f = influence coefficient due to bound circulation
A_s = influence coefficient due to trailing-edge circulation
A_w = influence coefficient due to separated wake circulation
c = wing chord
c_1 = coefficient in Eq. (8)
C_D = drag coefficient
C_L = lift coefficient
C_l = spanwise load distribution
C_p = pressure coefficient
f = vortex shedding frequency
F = normal force
h = panel vertical distance from x axis
P = pressure
p,q,r = angular velocity about x, y, and z axis, respectively
S = wing area
St = Strouhal number
t = time
U = wing forward velocity
u,v,w = induced velocity to the x, y, and z direction, respectively
$\bar{V}$ = velocity vector
V_u = upper shear velocity
V_l = lower shear velocity
x,y,z = wing coordinates
x_{sep} = chordwise location of separation line
α = angle of attack
Γ = circulation
Γ_f = wing bound circulation
Γ_s = separated wake circulation
Γ_w = trailing-edge wake circulation
ρ = density
ϕ = velocity potential

Introduction

THE high angle-of-attack aerodynamics of unswept wings has gained increased interest as a part of the safety oriented stall-spin alleviation research. These experimental studies[1-10] focused their effort on the understanding of general aviation aircraft aerodynamics beyond stall and on the development of leading-edge (LE) modifications to prescribe a preferred spanwise wing-stall pattern. Due to the complex three-dimensional nature of the separated flow over the wing, analytical methods are of limited use so that the results of some experiments and of some flow visualization patterns are still not completely understood.

The present study is an effort toward expanding analytical methods so that they can be applied to the flowfields of unswept wings that have local regions of separated flow. The procedure used employs a first-order large-scale vortex-lattice method to solve the three-dimensional flow. The objective of the method is to theoretically predict aspects of the flowfield which will provide an explanation of the flow visualization patterns (that are cellular in shape) that were observed[1-5] on the surface of stalled wings and to predict the wing pressure difference and the spanwise loadings.

Model

The proposed model for the unsteady partially separated flow of Fig. 1 is based on two stream patterns observed in the flow visualization studies. The first pattern[1-5] being a cellular type of three-dimensional (turbulent) separation where the cell shape is strongly dependent on the wing aspect ratio.[3] The schematic description of a representative surface-oil flow-visualization pattern for a wing with prescribed separation is

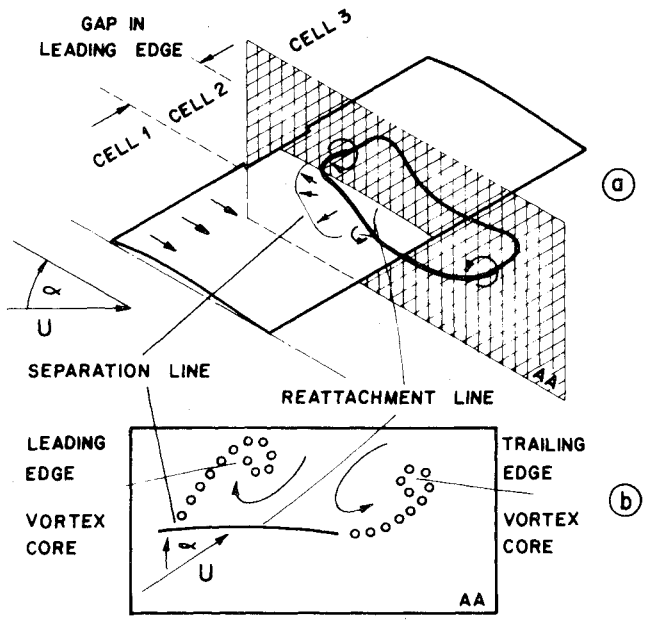

Fig. 1 Schematic of vortex model for the flow over a wing with prescribed midspan separation.

Presented as Paper 81-1264 at the AIAA 14th Fluid and Plasma Dynamics Conference, Palo Alto, Calif., June 23-25, 1981; submitted July 14, 1981; revision received March 17, 1982.

*Senior Lecturer, Mechanical Engineering. Member AIAA.

given in Fig. 2. Here, the early separation is prescribed at the middle of the wing span by means of a sharper leading edge that resulted in a gap in the top view of the wing leading edge.

The second type of pattern (Fig. 1b) observed in two-dimensional separated flows[11] where the periodic (Karman street) type of vortex shedding is dominant. In the simplified vortex model presented here, the vortex ring windward segment is placed into the time-average location of the separated vortex core, in the manner shown in Fig. 1a. Here (in Fig. 1), the flow is separated only behind the gap region, due to its sharper leading edge. However, for the modeling of separation in cells 1 and 3 similar vortex rings have to be added in these cells (see also, Fig. 3).

When constructing a vortex-lattice model (VLM), the influence of viscous effects dominating the separated flow should be properly accounted for. It is assumed, therefore, that the location of the separation line (which is a function of Reynolds number, airfoil curvature, and angle of attack) is known from flow visualization or local viscous flow calculations. In the present problem, however, this information is well-documented[1-10]; furthermore, in these studies flow separation was initiated in a predetermined manner.[4-10] When such information is provided, the wake rollup and forces on the airfoil can be investigated by means of unsteady potential theory. This extension (unsteady) is necessary since beyond stall, periodic flow patterns are observed[11] but the existence of such flow over a wide range of angle of attack was not established in most experimental works.[1-10] The basic assumptions of this model are that the flow is incompressible, irrotational, and homogeneous over the whole fluid region excluding the wing and its wake.

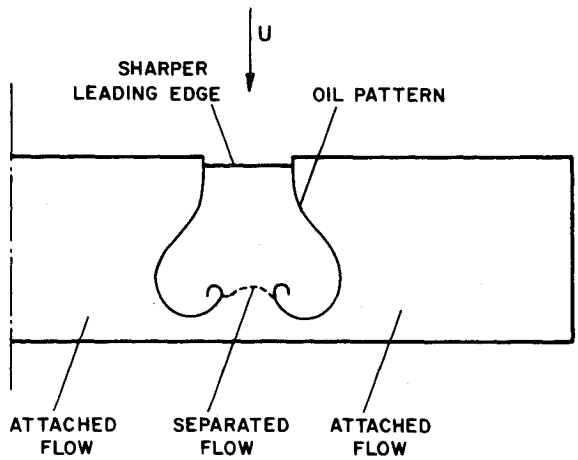

Fig. 2 Schematic description of the surface-oil flow-visualization pattern due to the separated flow behind the gap region.

Under these conditions the existence of a velocity potential ϕ can be established, whereas the continuity equation becomes

$$\nabla^2\phi = 0 \tag{1}$$

The general solution of Eq. (1), including the unsteady boundary conditions, is a sum of doublet and source distribution.[12] The thickness effect represented by the source solution is not investigated here whereas the lifting thin-wing problem will be solved by VLM. The first boundary condition for Eq. (1) requires that no fluid will flow through the wing surface; thus,

$$\frac{\partial\phi}{\partial z}\bigg|_{\text{on wing}} = (U-ry)\left(\frac{\partial h}{\partial x} - \sin\alpha\right) - qx + py + \frac{\partial h}{\partial t} \tag{2}$$

where $U=U(t)$ is the momentary flight velocity, $z=h(x,y,t)$ is the momentary camber line, and (p,q,r) are the angular velocity components. Furthermore, it is required that the velocity induced by the wing decays far from the wing and its wake

$$\nabla\phi = 0 \qquad (\text{as } |x|, |y|, |z| \to \infty) \tag{3}$$

The wake and wing circulation must fulfill Kelvin's law; that is, the overall circulation (Γ) generated in the flow must be

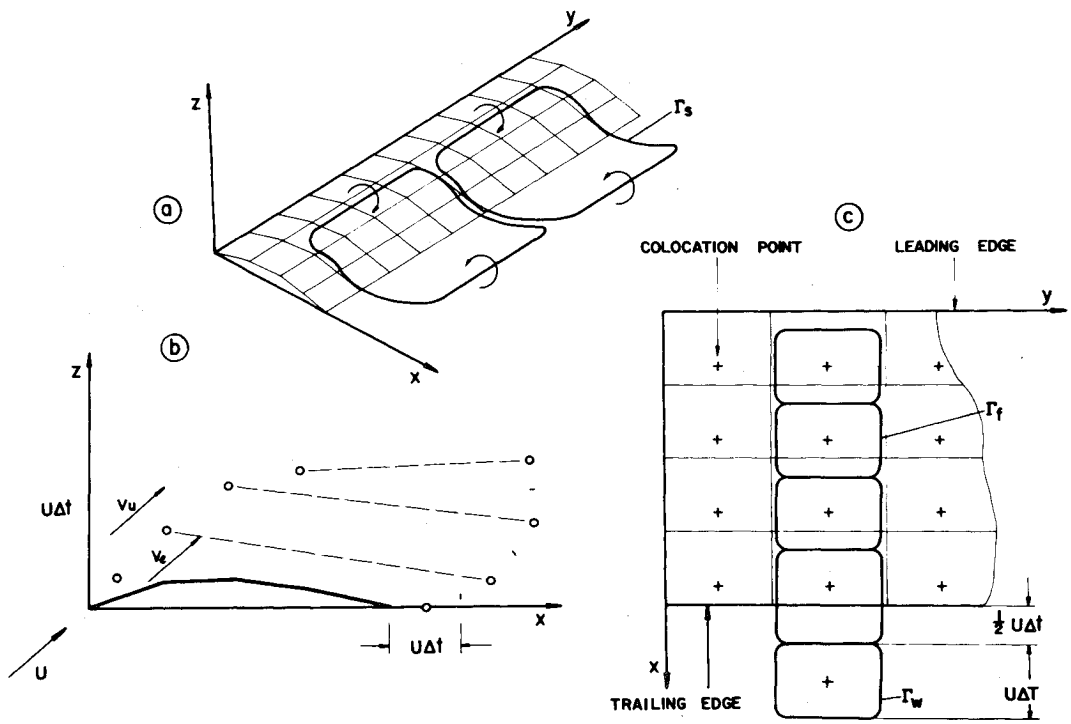

Fig. 3 Vortex panel and wake geometry.

zero

$$\frac{d\Gamma}{dt} = 0 \quad \text{(for all } t\text{)} \tag{4}$$

Vortex Solution

The problem stated by Eqs. (1-4) is solved by dividing the wing planform into panels as shown in Fig. 3a. Each panel consists of a vortex ring with its front spanwise segment placed at the panel quarter length, and its rear segment placed one panel chord length downstream. The collocation point is placed at the panel three-quarter chord, at the center of the vortex ring (Fig. 3c).

By selecting the vortex ring representation, Eqs. (1) and (3) already are fulfilled since the vortex is a fundamental solution of the Laplace equation. Furthermore, the closed vortex form ensures the existence of the Kelvin condition Eq. (4), and the aforementioned placing of the vortex ring at each panel fulfills the Kutta condition; thus, for the complete solution, only boundary condition Eq. (2) is left, which in terms of the unknown bound vortices Γ_{f_i} will have the following form.

$$\{w\} = [A_f]\{\Gamma_f\} + [A_w]\{\Gamma_w\} + [A_s]\{\Gamma_s\} \tag{5a}$$

$$\{w\} = \begin{Bmatrix} \frac{\partial\phi}{\partial z_1} \\ \vdots \\ \frac{\partial\phi}{\partial z_n} \end{Bmatrix}; \quad \{\Gamma_f\} = \begin{Bmatrix} \Gamma_{f_1} \\ \vdots \\ \Gamma_{f_n} \end{Bmatrix}$$

$$\{\Gamma_w\} = \begin{Bmatrix} \Gamma_{w_1} \\ \vdots \\ \Gamma_{w_m} \end{Bmatrix}; \quad \{\Gamma_s\} = \begin{Bmatrix} \Gamma_{f_1} \\ \vdots \\ \Gamma_{s_\ell} \end{Bmatrix} \tag{5b}$$

Here the first term in Eq. (5a) represents the contribution of the wing bound circulation Γ_f to the downwash velocity, while the second and third terms stand for the contribution of trailing-edge wake (Γ_w) and separated wake (Γ_s), respectively.

The downwash vector $\{w\}$ is calculated at the collocation point of each panel by Eq. (2) and the influence matrix coefficients $[A_f]$, $[A_w]$, and $[A_s]$ are obtained by using the Biot-Savart law to calculate the induced velocities of the vortex filaments. If wing geometry is not varying during flight (e.g., flap deflection, etc.), then the matrix $[A_f]$ is calculated only once at the beginning of the calculation procedure. The order n of the vectors corresponds to the number of panels, whereas m and l are the number of wake elements that increases with each time interval. In Eq. (5a) the unknown $\{\Gamma_f\}$ is to be calculated, whereas the strength of vortices shed from the trailing edge (TE) $\{\Gamma_w\}$ and from the leading edge $\{\Gamma_s\}$ are known from previous time steps.

Separated Vortex Wake

In order to allow the modeling of the separated flow about wings having unswept LE, the separated flow vortex element has been introduced. In practice, empirical input or flow visualization data will provide the information at which panel (row and column) the separation lines will cross. In Fig. 3b separation occurs from the first row (to simulate LE separation), thus the spanwise vortex filament location will be in the middle of the distance covered during the latest time step by the same panel leading edge. This vortex will form a ring when connected to the vortex placed in the middle of the path covered by the TE during the same time interval. The choice of the time step Δt must not be smaller than the equivalent panel chord length Δc; thus,

$$\Delta t_{\min} U/\Delta c \simeq 1 \tag{6}$$

When the wing bound circulation is represented by a large number of panels or when a continuous bound vortex distribution is used,[13] then the time steps can be smaller as in Fig. 1b and the time-dependent wake rollup can be calculated with more details. When, however, simplicity is preferred, and only the time-average forces are to be investigated, then the large-scale effect can be accounted for by placing one vortex in the average vortex core as shown in Figs. 1a and 3a. This is done by simply increasing the time step and the most preferred time interval is the one which corresponds to the Strouhal frequency (the value of 0.20 for the Strouhal number was used), at the poststall conditions,

$$\Delta t = \frac{1}{f} = \frac{c\sin\alpha}{StU} \tag{7}$$

However, time intervals much larger than ($\Delta tU/c = 1$) are not recommended.

The strength of the separated wake elements $\{\Gamma_s\}$ at the latest time interval is calculated by the shear velocity calculation

$$\frac{d\Gamma_{s_i}}{dt} = \frac{d}{dt}\oint \bar{V} ds = \frac{d}{dt}(V_u ds - V_\ell ds) \simeq \frac{c_1}{2}(V_u^2 - V_\ell^2) \tag{8}$$

The validity of this simple expression was shown experimentally by Fage and Johansen[15] and was used since in numerous numerical calculations[13] (with the value of 0.6 for the circulation reduction factor c_1). The upper and lower velocities (V_u, V_ℓ) are measured above and under the shear layer as shown in Fig. 3b. In practice, the lower velocity can be measured at the separated panel collocation point and the upper velocity is measured above the separated wake in a distance where the effect of vortex wake discretization is minimal (0.3-0.4c above separated vortex wake).

Equation (8) determines the strength of the latest Γ_s element shed, thus, combined with Eq. (5a) provides n equation with n unknown Γ_{f_i} that can be solved at each time interval.

The deformation of the wake sheet is analyzed by moving each wake vortex tip by the amount $(\Delta x, \Delta y, \Delta z)_i$ such that

$$\begin{Bmatrix} \Delta x \\ \Delta y \\ \Delta z \end{Bmatrix}_i = \begin{Bmatrix} u \\ v \\ w \end{Bmatrix}_i \Delta t \tag{9}$$

where $(u,v,w)_i$ is the wing-wake induced velocity at each vortex tip. The calculation of these velocities is done using the Biot-Savart law in a similar manner to Eq. (5a).

When the solution of the flow [Eqs. (1-4)] is completed, for a certain time interval, the resulting aerodynamic forces are calculated

$$\Delta P_i \simeq 2\rho\left[(U - ry_i)\frac{\partial\phi_i}{\partial x} + \frac{\partial\phi_i}{\partial t}\right] \tag{10}$$

and the normal force contribution ΔF_i of each panel with the chord length $\Delta x_i = x_i - x_{i-1}$ and width Δy_i in terms of its bound vorticity Γ_{f_i} is

$$\frac{\Delta F_i}{\Delta y_i} = 2\rho\left[(U - ry_i)\int_{x_{i-1}}^{x_i}\frac{\partial\phi}{\partial x}dx + \int_{x_{i-1}}^{x_i}\frac{\partial}{\partial t}\int_0^x \frac{\partial\phi}{\partial x}dx dx\right]$$

$$\simeq \rho\left\{(U - ry_i)\Gamma_{f_i} + \frac{\partial}{\partial t}\left(\sum_{k=1}^{i-1}\Gamma_{f_k}\Delta x_k + \Gamma_{f_i}\frac{\Delta x_i}{2}\right)\right\} \tag{11}$$

The summation

$$\sum_{k=1}^{i-1} \Gamma_{f_k}$$

is a result of the

$$\int_0^x \frac{\partial \phi}{\partial x}$$

term and, therefore, must start at the leading-edge panel, ahead of the one for which ΔF_i is to be calculated. The momentary lift and drag coefficients are calculated by summing up the contribution of all the panels

$$C_L = \frac{1}{\frac{1}{2}\rho U^2 S} \sum_{i=1}^{n} \Delta F_i \cos\alpha_i \tag{12}$$

$$C_D = \frac{1}{\frac{1}{2}\rho U^2 S} \sum_{i=1}^{n} \Delta F_i \sin\alpha_i \tag{13}$$

Here, S is the wing area and α_i the panel angle of attack. The thin wing leading-edge suction force was neglected here, since at angles of attack near separation its contribution to the drag direction is small, if any.

The preceding mathematical representation of the flowfield requires a starting type of solution. Thus, the motion of the wing can describe a general unsteady path[12] or a stationary position[13,14] but, in either case, the airfoil motion must be started from rest. When a steady-state condition is to be investigated (as in the present work), the required path traveled by the foil, until the final calculational interval, may vary with wing aspect ratio. This length is in the order of 2-3 chords for delta wings with aspect ratio of 1 and up to 10-20 chord lengths for a rectangular wing with infinite span. The solution procedure at each time interval Δt consists of moving the wing to its new location, shedding the separated wake and trailing-edge vortex rings with the strength calculated at the previous time step, and then calculating the geometrical downwash of Eq. (2) at each collocation point. The boundary condition of Eq. (5a) is solved next providing the bound circulation strength Γ_{f_i}, and then the wake deformation is calculated by moving each vortex tip location according to Eq. (9). The planform lift and drag is obtained finally by Eqs. (11-13) and, after doing so, the wing can be advanced to its new location and then the whole procedure is repeated.

Rectangular Planform with Prescribed Separation

The search for an aerodynamically stall-spin resistant aircraft configuration focused the attention on developing wing planforms such that their separation pattern will develop in a predetermined manner.[2-10] Consequently, sudden lift losses are excluded and a "flat top" lift curve is desired. This eliminates the stall-spin causing large rolling moments due to the early stalling of one wing before the other, when the aircraft is flying in a near stall condition. The separated region (for a given high angle of attack before stall) was prescribed by several methods. At NASA Langley, the leading-edge droop concept[2,5-7] was adopted to protect the wing sections where the attached flowfield was required for the higher angles of attack. At these regions also LE slats[4,5] were used, or larger radii LE gloves[2] as in the experiments at NASA Ames.[8-10] Also, the LE spoiler[10] for prescribing early separation at a given location was used successfully for this purpose.

On the other hand, basic flow visualization data[1-3] showed the existence of cellular patterns above rectangular, unswept wings with $\mathcal{R}$ in the order of 5-10, under partial or fully stalled conditions. The major reason for the development of the mathematical model of this paper is to suggest a tool for the analysis of the interaction between the cellular separation pattern above unswept wings and the wing planform and to study the forced separation patterns prescribed by the aforementioned LE modifications. Furthermore, by introducing this model, a logical order is introduced into the data reduction of the oceanful of experimental data generated on these wing planforms.

Since the geometrical location of prescribed separation lines on the wing is well-documented throughout the whole range of the presented experiments, the application of this mathematical model was made possible. In more general cases, however, an interacting viscous computational code can provide the separation line geometry for the potential model or else experimental information is required. The unsteady nature of the model enables the study of phenomena such as buffeting[13] (when separation point location and range of motion is known), or the detailed calculation of wake rollup pattern as shown in Fig. 1b; but in these cases small time steps are required ($0.01 \le \Delta t U/c \le 0.1$). When the time-average forces are to be studied, then larger time intervals can be used as determined by Eq. (7) and the stationary model (Figs. 1 and 3) will show resemblance to the flow visualization photographs of Winkelmann et al.[2,3] In these situations the time-dependent separation line oscillations are rather small and the model consisting of a large-scale vortex core above the wing, as used here, is sufficient. A more detailed unsteady wake rollup survey and flow visualization, for a wide range of Reynolds number and angle of attack, is a necessity for a deeper understanding of the poststall aerodynamics of wings.

Figure 4 shows a comparison of calculated and measured[10] lift coefficients for a rectangular wing having an aspect ratio of 7.5 at $Re = 1.5 \times 10^6$. The separation line location was obtained by tuft studies in the NASA Ames 7×10-ft wind tunnel.[10] The mathematical model for the semispan wing consisted of a 13×4 panel lattice and, therefore, the separation line could be located only at five chordwise locations. Here the large-scale separated vortex model of Fig. 3 was used and the existence of two major vortex rings was assumed (as in Ref. 3 for $\mathcal{R} \simeq 6$). Calculation time for a given angle of attack on a CDC 7600 computer was about 10-50 s. For the range of angle of attack of $9 < \alpha < 15$ deg the trailing-edge separation starts to develop (with the airfoil section NACA 63_2-415) as observed by the tufts motion during the wind tunnel test. To account for this effect the trailing-edge panel row was allowed to separate, as indicated by Fig. 4b where the separation line location x_{sep} can have only the values of 0., 0.25, 0.50, 0.75, and 1.00 (since only four chordwise panels were used).

From angle of attack $\alpha = 15$ deg up to 19 deg the separation line moves gradually forward, up to the midchord causing the lift curve to bend. In the present calculation only one panel existed within this region and, therefore, only two calculated points are shown ($\alpha = 15$ deg, $x_{sep} = 0.75$ and $\alpha = 19$ deg, $x_{sep} = 0.50$). In Fig. 5, the chordwise pressure difference $[\Delta C_p = \Delta P/(0.5\rho U^2 1c)]$ at the wing centerline ($y/b = 0$) is shown for two typical data points of Fig. 4. The first is the attached flow condition ($\alpha = 9$ deg) and even though only four chordwise panels were used, the typical chordwise pressure distribution for the linear flow is observed. The other curve of Fig. 5 shows the pressure distribution at the fully separated ($\alpha = 25$ deg) case where the lift loss at the front row is due to the large vortex core above the wing.

The comparison of experimental lift curve with the calculated results for the wing with the LE modification is shown in Fig. 6. The wing LE was protected by a glove[10] (as shown by the insert in Fig. 6) which actually increased LE radii by adding the front section of a 17% thick GAW-1 airfoil as explained in Ref. 10. The lift curve was linear up to $\alpha = 11$ deg, after which rapid separation developed within the gap region. This development ends at $\alpha = 13$ deg with the complete LE separation. The mathematical model used was as

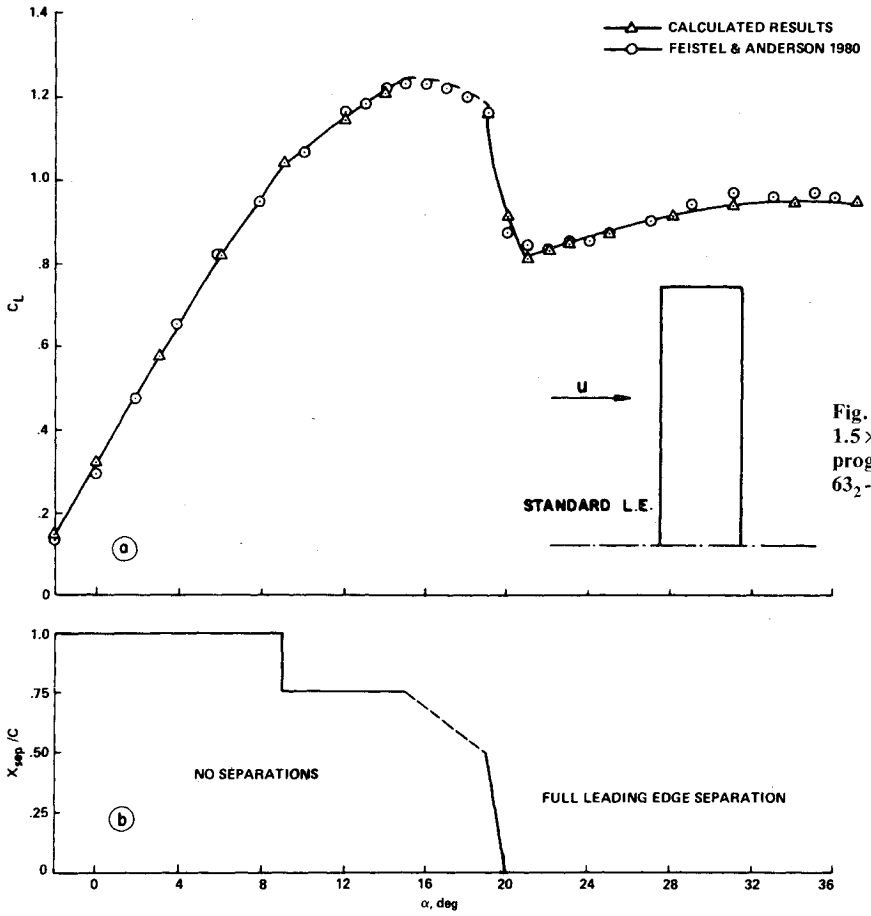

Fig. 4 Calculated and experimental ($Re = 1.5 \times 10^6$) lift curve and trailing-edge separation progression of a rectangular planform (NACA 63_2-415 section, $AR = 7.5$).

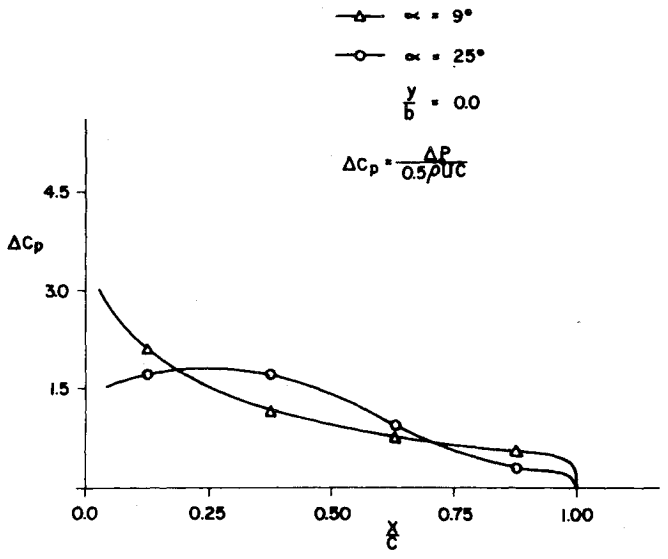

Fig. 5 Calculated chordwise pressure distribution for attached and separated flow (at wing midspan).

shown in Fig. 1; and a single vortex ring was present behind the gap with the sharper LE. At an angle of attack of $\alpha = 15$ deg the inboard separation vortex ring starts to develop and its motion x_{sep} as observed by tuft studies is shown in Fig. 6b. At about 20 deg the inboard separated vortex ring reaches the LE, whereas the outboard separation starts to develop. This separation, however, does not reach the fully separated condition even at $\alpha = 36$ deg where in practice the outboard LE and wing tip flow is still attached. It is interesting to compare the C_L values of Fig. 4 and Fig. 6 above $\alpha = 32$ deg. Even when comparing the results presented in Ref. 10 for the wing with the full LE glove (no LE gaps), the results at this range are similar to those in Fig. 4. This is probably a result of the instability of the LE separated vortex line which immediately tends to break up into vortex rings, resulting in a fast forward travel of the separation line. When, however, wing separation pattern is carefully prescribed, its forward motion is gradual and the vortex break-up into rings is not spontaneous. Therefore, the forward travel of the separation line has less "inertia" and the abrupt lift losses are eliminated.

When comparing the experimental results of the basic 63_2-415 airfoil (Fig. 4) and the wing with the continuous glove[10] to the results of Fig. 6, the following mechanism for the development of a flat-top lift curve is suggested. The early separation at the gap is reducing lift (compared to the full glove configuration) and a lower maximal lift is obtained. At the higher angles of attack $26 > \alpha > 20$ deg separation develops gradually and lift losses are excluded. Therefore, if due to asymmetric flight one of the aircraft wings stalls first, the resulting spin aggravating rolling moments will be small. In the smooth LE wing case, however, the beginning of the separation is delayed slightly and higher maximal lift coefficients are obtained; but, as stated, here the stall is faster and accompanied with larger lift losses. In terms of rolling moments when one of the aircraft wings is stalled, this can be a much harder situation to control.

Figure 7 shows the pressure difference ΔC_p, in the middle of the gap section for the case with separated flow at this region and for the theoretical case of completely attached flow (both at $\alpha = 14$ deg). The large lift loss at the first panel row is a result of the downwash induced by the narrow separated vortex ring (Fig. 1); the resolution of this pressure distribution can be improved by using a more dense panel grid (only 4 chordwise panels were used). Experimental pressure

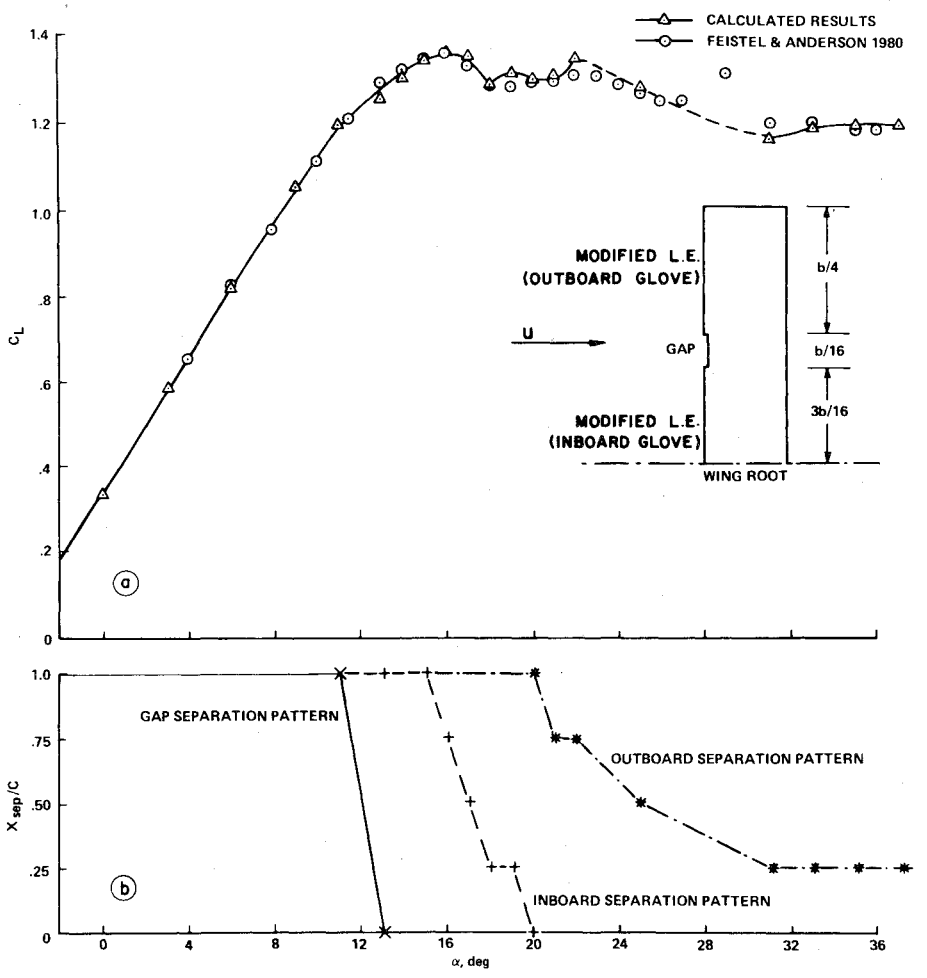

Fig. 6 Calculated and experimental lift curve and trailing-edge separation progression of a rectangular planform with leading-edge modification ($\mathcal{A}R = 7.5$, $Re = 1.5 \times 10^6$).

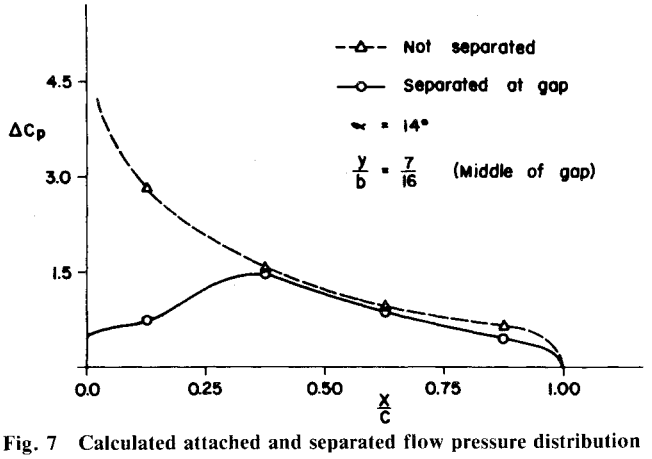

Fig. 7 Calculated attached and separated flow pressure distribution in the gap section.

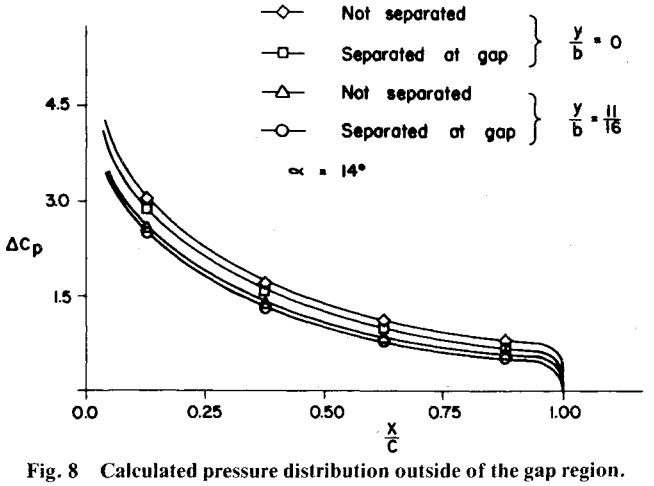

Fig. 8 Calculated pressure distribution outside of the gap region.

data[2,4,5] for symmetric airfoils does not show this effect but further experiments with airfoils having dropped LE (63_2-415) can clarify this problem.

Figure 8 compares the theoretical chordwise pressure in both sides of the gap section for a hypothetical fully attached flow and for the prescribed separation (in gap) case. It is shown that the presence of the separated vortex ring behind the gap reduces somewhat the effective section angle of attack in both sides and, in practice, this delays the separation of these sections. This means that there is a limited potential effect indicating that such prescribed separation does have a delaying effect on the separation of the wing's other sections.

Figure 9 was drawn in order to gain some insight into the mechanism of prescribed separation. The two spanwise locations of the gap do not change much the spanwise loading C_l and the slightly smaller tip load indicates that a closer gap to wing tip will result in a slightly later separation initiation at the wing tip. This trend was shown experimentally by Feistel et al.[10] where the outboard gap geometry resulted in a later separation of the inboard section. Furthermore, due to the larger area of the inboard region, beyond stall higher destabilizing rolling moments were measured (since one wing stalled before the other). Thus higher C_{Lmax} was obtained but then the loss in this wing section lift was not eliminated and the flat-top lift curve was not achieved.

It is concluded, therefore, that for each wing when flat-top lift curve is desired, the gap size and spanwise location is a function of wing geometry (twist, taper, etc.) and must be

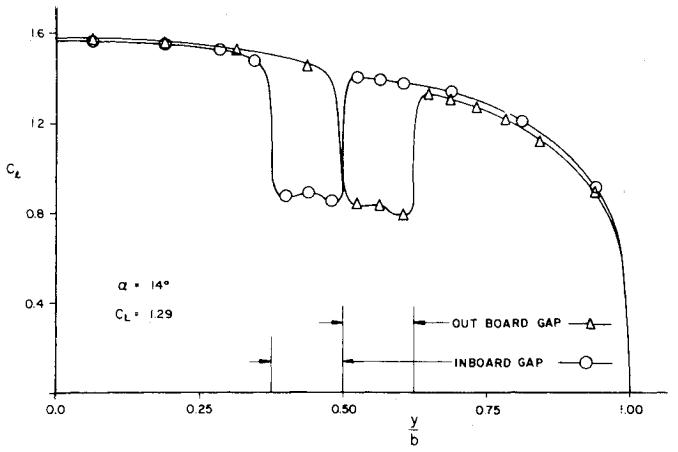

Fig. 9 Spanwise load distribution for two spanwise gap locations.

carefully placed. For rectangular untwisted planforms, a position which is slightly inside of the midspan is preferred.

Furthermore, leading-edge discontinuity must not be placed such that the natural cellular separation structure will be affected. Therefore, the division of wings having a high aspect ratio (of $6 \div 8$) into three cells (two discontinuities in LE) as reported by Refs. 8-10 is more predictable than the division into two primary cells (only one discontinuity in LE) as reported by Refs. 5-7.

Concluding Remarks

The complex flowfield about separated, unswept leading-edge wings was analyzed by a first-order vortex-lattice method. Calculated lift data, based on experimentally known separation line location, was in agreement with wind tunnel results. The analysis of wing planforms with prescribed separation showed the possibility of obtaining a flat-top type lift curve that will reduce aircraft rolling moments when one wing is stalled prematurely. Future extension of this method might include a viscous flow solution to provide the motion and location of flow separation line. The extension of experimental information is also recommended to enable future developments such as active separation control. This requires the detailed wing surface and wake pressure measurement of partially stalled wings and the careful documentation of vortex development and motion, through a wide range of angle of attack.

References

[1] Moss, G. F. and Murdin, P. M., "Two Dimensional Low-Speed Tunnel Tests on the NACA 0012 Section Including Measurements Made During Pitching Oscillation at the Stall," RAE-TR 68104, May 1968.

[2] Winkelmann, A. E., Barlow, J. B., Saini, J. K., Anderson, J. D. Jr., and Jones, E., "The Effect of Leading Edge Modifications on the Post Stall Characteristics of Wings," AIAA Paper 80-0199, Pasadena, Calif., 1980.

[3] Winkelmann, A. E. and Barlow, J. B., "Flowfield Model for a Rectangular Planform Wing beyond Stall," *AIAA Journal*, Vol. 18, Aug. 1980, pp. 1006-1008.

[4] Meznarsic, V. F. and Gross, L. W., "An Experimental Investigation of a Wing with Controlled Mid-Span Flow Separation," AIAA Paper 80-1804, Anaheim, Calif., 1980.

[5] Johnson, J. L. Jr., Newsom, W. A., and Satran, D. R., "Full-Scale Wind Tunnel Investigation of the Effects of Wing-Leading-Edge Modification on the High Angle-of-Attack Aerodynamic Characteristics of a Low-Wing General Aviation Airplane," AIAA Paper 80-1844, Anaheim, Calif., 1980.

[6] DiCarlo, D. J. and Johnson, J. L. Jr., "Exploratory Study of the Influence of Wing Leading-Edge Modifications on the Spin Characteristics of a Low-Wing Single-Engine General Aviation Airplane," AIAA Paper 79-1837, N.Y., N.Y., 1979.

[7] DiCarlo, D. J., Stough, H. P. III, and Patton, J. M. Jr., "Effects of Discontinuous Drooped Wing Leading-Edge Modifications on the Spinning Characteristics of a Low-Wing General Aviation Airplane," AIAA Paper 80-1843, Anaheim, Calif., 1980.

[8] Kroeger, R. A. and Feistel, T. W., "Reduction of Stall-Spin Entry Tendencies Through Wing Aerodynamic Design," presented at Wichita, Kan., SAE Paper 760481, April 1976.

[9] Feistel, T. W. and Anderson, S. B., "A Method for Localizing Wing Flow Separation at Stall to Alleviate Spin Entry Tendencies," AIAA Paper 78-1476, Los Angeles, Calif., 1978.

[10] Feistel, T. W., Anderson, S. B., and Kroeger, R. A., "Alleviation of Spin-Entry Tendencies Through Localization of Wing-Flow Separation," *Journal of Aircraft*, Vol. 18, Feb. 1981, pp. 69-75.

[11] McAlister, K. W. and Carr, L. W., "Water Tunnel Experiments on an Oscillating Airfoil at $R_e = 21{,}000$," NASA TN-2502, 1978.

[12] Katz, J., "Method for Calculating Wing Loading During Maneuvering Flight Along a Three-Dimensional Curved Path," *Journal of Aircraft*, Vol. 16, Nov. 1979, pp. 739-741.

[13] Katz, J., "A Discrete Vortex Method for the Unsteady Separated Flow over an Airfoil," *Journal of Fluid Mechanics*, Vol. 102, 1981, pp. 315-328.

[14] Levin, D. and Katz, J., "A Vortex-Lattice Method for the Calculation of the Nonsteady Separated Flow over Delta Wings," *Journal of Aircraft*, Vol. 18, 1981, pp. 1032-1037.

[15] Fage, A. and Johansen, F. C., "On the Flow of Air Behind an Inclined Flat Plate of Infinite Span," *Proceedings of the Royal Society*, Ser. A, Vol. 116, 1927, pp. 170-197.